PUBLICATIONS OF THE ASTRONOMICAL SOCIETY OF THE PACIFIC, **123**:547–554, 2011 May

WASP-41b: A Transiting Hot Jupiter Planet Orbiting a Magnetically Active G8V Star

P. F. L. MAXTED,[1] D. R. ANDERSON,[1] A. COLLIER CAMERON,[2] C. HELLIER,[1] D. QUELOZ,[3] B. SMALLEY,[1] R. A. STREET,[4] A. H. M. J. TRIAUD,[3] R. G. WEST,[5] M. GILLON,[6] T. A. LISTER,[4] F. PEPE,[3] D. POLLACCO,[7] D. SÉGRANSAN,[3] A. M. S. SMITH,[1] AND S. UDRY[3]

Received 2010 December 6; accepted 2011 March 3; published 2011 April 19

ABSTRACT. We report the discovery of a transiting planet with an orbital period of 3.05 days orbiting the star TYC 7247-587-1. The star, WASP-41, is a moderately bright G8 V star ($V = 11.6$) with a metallicity close to solar ($[\mathrm{Fe/H}] = -0.08 \pm 0.09$). The star shows evidence of moderate chromospheric activity, both from emission in the cores of the Ca II H and K ines and photometric variability with a period of 18.4 days and an amplitude of about 1%. We use a new method to show quantitatively that this periodic signal has a low false-alarm probability. The rotation period of the star implies a gyrochronological age for WASP-41 of 1.8 Gyr with an error of about 15%. We have used a combined analysis of the available photometric and spectroscopic data to derive the mass and radius of the planet ($0.92 \pm 0.06\ M_{\mathrm{Jup}},\ 1.20 \pm 0.06\ R_{\mathrm{Jup}}$). Further observations of WASP-41 can be used to explore the connections between the properties of hot Jupiter planets and the level of chromospheric activity in their host stars.

1. INTRODUCTION

There is continued interest in finding bright stars that host transiting exoplanets, because they can be accurately characterized and studied in some detail; e.g., the mass and radius of the planet can be accurately measured. This gives us the opportunity to explore the relationships between the properties of the planet and its host star: e.g., the orbital eccentricity, the composition and spectral type of the star, the age of the system, etc. Given the wide variety of transiting planets being discovered and the large number of parameters that characterize them, statistical studies will require a large sample of systems to identify and quantify the relationships between these parameters. These relationships can be used to test models of the formation, structure, and evolution of short-period exoplanets.

Here, we report the discovery by the Wide Angle Search for Planets (WASP) survey of a planetary mass companion to the star TYC 7247-587-1. We find that the star is a G8 V star showing moderate chromospheric activity. The planet, WASP-41b, is a typical hot Jupiter planet with an orbital period of 3.05 days.

[1] Astrophysics Group, Keele University, Staffordshire, ST5 5BG, UK.
[2] SUPA, School of Physics and Astronomy, University of St. Andrews, North Haugh, Fife, KY16 9SS, UK.
[3] Observatoire astronomique de l'Université de Genève 51 ch. des Maillettes, 1290 Sauverny, Switzerland.
[4] Las Cumbres Observatory, 6740 Cortona Dr. Suite 102, Santa Barbara, CA 93117, USA.
[5] Department of Physics and Astronomy, University of Leicester, Leicester, LE1 7RH, UK.
[6] Institut d'Astrophysique et de Géophysique, Université de Liège, Allée du 6 Août, 17, Bat. B5C, Liège 1, Belgium.
[7] Astrophysics Research Centre, School of Mathematics & Physics, Queen's University, University Road, Belfast, BT7 1NN, UK.

2. OBSERVATIONS

The WASP survey is described in Pollacco et al. (2006) and Wilson et al. (2008), while a discussion of our candidate selection methods can be found in Collier Cameron et al. (2007), Pollacco et al. (2008), and references therein.

The star TYC 7247-587-1 (WASP-41, 1SWASP J124228 .50-303823.5) was observed 6767 times by one camera on the WASP-South instrument from 2007 January 20 to 2007 June 22. A further 5637 observations were obtained with the same camera from 2008 January 17 to 2008 May 28.

The WASP-South light curves of WASP-41 show transitlike features, with a depth of approximately 0.02 mag recurring with a 3.05 day period (Fig. 1). These were independently detected in the WASP-South photometry from the two seasons using the detrending and transit detection methods described in Collier Cameron et al. (2007), which was taken as good evidence that the periodic transit signal was real. The spectral type of the star was estimated to be approximately G8, based on the catalog photometry available for this star at the time. The duration and depth of the transit are consistent with the hypothesis that they are due to the transit of a planetlike companion to a main-sequence G8 star, and the WASP-South light curves show no indication of any ellipsoidal variation due to the distortion of the star by a massive companion.

We obtained 22 radial velocity measurements during the interval of 2010 January 3 to 2010 August 5 with the fiber-fed

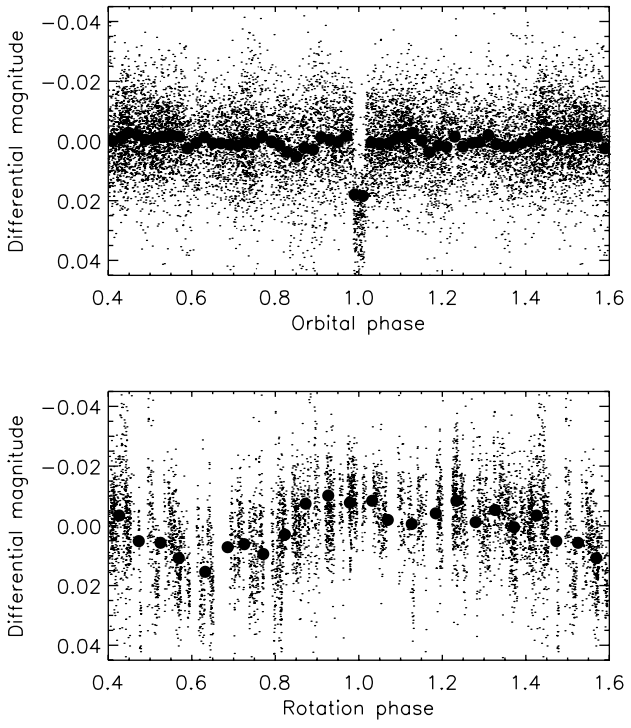

FIG. 1.—WASP-South photometry of WASP-41. Raw data are plotted using small points, and phase-binned data are plotted using filled circles. *Top*: All data plotted as a function of the orbital phase with period $P = 3.0524$ days. *Bottom*: Data from 2008 plotted as a function of the rotation phase with period $P_{\rm rot} = 18.4$ days.

Coralie spectrograph on the Euler 1.2 m telescope located at La Silla, Chile. The spectra were obtained with an exposure time of 30 minutes and have a typical signal-to-noise ratio of 25–30. Accurate wavelength calibration is ensured by the simultaneous observation of a thorium-argon arc in a second fiber feed to the spectrograph. Details of the instrument and data reduction can be found in Queloz et al. (2000) and references therein. The RV measurements were performed using cross-correlation against a numerical mask generated from a G2-type star and are given in Table 1, where we also provide the bisector span (BS), which measures the asymmetry of the cross-correlation function (Queloz et al. 2001). The standard error of the bisector span measurements is $2\sigma_{\rm RV}$.

We also obtained photometry of TYC 7247-587-1 and other nearby stars on 2010 June 23 using the LCOGT 2.0 m Faulkes Telescope South (FTS) at Siding Spring Observatory. The Merope camera we used has an image scale of $0.279''$ pixel^{-1} when used in the 2×2 binning mode we employed. We used a Panoramic Survey Telescope and Rapid Response System (Pan-STARRS[8]) z-band filter to obtain 210 images covering one transit. These images were processed in the standard way with IRAF[9] using a stacked bias image, dark frame, and sky flat. The DAOPHOT photometry package (Stetson 1987) was used to perform object detection and aperture photometry for WASP-41 and several comparison stars in the $5' \times 5'$ field of view of the instrument. Observations were interrupted by poor weather, so there are no observations during the egress phase of the transit. These data are sufficient to confirm that the transitlike features seen in the WASP-South data are due to the star TYC 7247-587-1 and to provide better measurements of the depth of the transit than is possible from the WASP-South data (Fig. 2).

All photometric data presented in this article are available from the NStED database.[10]

TABLE 1
RADIAL VELOCITY MEASUREMENTS FOR WASP-41

BJD 2,450,000	RV (km s^{-1})	$\sigma_{\rm RV}$ (km s^{-1})	BS (km s^{-1})
5200.8101	3.1691	0.0076	−0.0168
5290.8090	3.3837	0.0070	−0.0323
5293.8035	3.4106	0.0087	−0.0369
5294.8225	3.2084	0.0077	−0.0193
5295.7751	3.1732	0.0069	−0.0048
5296.7550	3.3926	0.0070	−0.0240
5297.8185	3.2263	0.0083	−0.0076
5298.7732	3.1696	0.0073	−0.0303
5300.8114	3.2652	0.0084	−0.0067
5301.8036	3.1611	0.0088	+0.0268
5305.7269	3.3935	0.0071	−0.0239
5306.7188	3.3411	0.0072	−0.0043
5311.8040	3.3486	0.0088	−0.0356
5317.5927	3.3310	0.0101	−0.0144
5323.6579	3.2985	0.0073	−0.0193
5326.6585	3.2569	0.0071	+0.0065
5327.6832	3.4099	0.0133	−0.0278
5362.4677	3.1436	0.0123	+0.0065
5375.5148	3.2806	0.0080	−0.0043
5388.5621	3.4714	0.0092	−0.0490
5410.5201	3.3512	0.0083	−0.0182
5414.4912	3.1813	0.0083	−0.0024

3. WASP-41 STELLAR PARAMETERS

The 17 individual Coralie spectra of WASP-41 available up to 2010 May were co-added to produce a single spectrum with a signal-to-noise ratio of ≈70:1. The standard pipeline reduction products were used in the analysis.

The analysis was performed using the methods given in Gillon et al. (2009). The Hα line was used to determine the effective temperature ($T_{\rm eff}$), while the Na I D and Mg I b lines were used as surface gravity ($\log g$) diagnostics. The parameters obtained from the analysis are listed in Table 2. The elemental

[8] See http://pan-starrs.ifa.hawaii.edu/public/design-features/cameras.html.

[9] IRAF is distributed by the National Optical Astronomy Observatory, which is operated by the Association of Universities for Research in Astronomy (AURA) under cooperative agreement with the National Science Foundation.

[10] See http://nsted.ipac.caltech.edu.

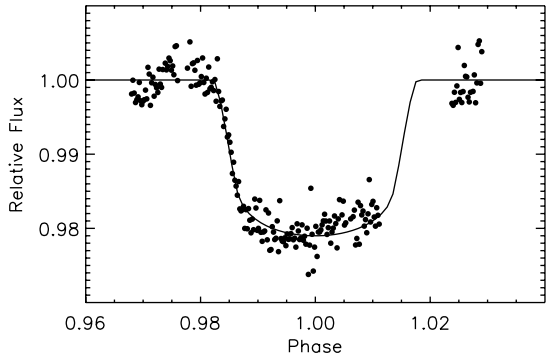

FIG. 2.—Faulkes Telescope South z-band photometry of WASP-41 (*filled circles*) with the model fit described in § 5 (*solid line*).

abundances were determined from equivalent width measurements of several clean and unblended lines. A value for microturbulence (ξ_t) was determined from Fe I using the method of Magain (1984). The quoted error estimates include those given by the uncertainties in $T_{\rm eff}$, $\log g$, and ξ_t, as well as the scatter due to measurement and atomic data uncertainties.

The projected stellar rotation velocity ($v \sin i$) was determined by fitting the profiles of several unblended Fe I lines. A value for macroturbulence ($v_{\rm mac}$) of 2.3 ± 0.3 km s^{-1} was assumed, based on the tabulation by Gray (2008), and an instrumental FWHM of 0.11 ± 0.01 Å, determined from the telluric lines around 6300 Å. A best-fitting value of $v \sin i = 1.6 \pm 1.1$ km s^{-1} was obtained.

We observe emission lines in the cores of the Ca II H and K lines in our spectrum of WASP-41 (Fig. 3). We estimate a spectral index $\log R'_{\rm HK} \approx -4.67$ from this spectrum (Noyes et al. 1984), but note that a transformation for measurements made with the Coralie spectrograph to a standard system does not yet exist.

TABLE 2

STELLAR PARAMETERS OF WASP-41 FROM SPECTROSCOPIC ANALYSIS

Parameter	Value
$T_{\rm eff}$	5450 ± 150 K
$\log g$	4.4 ± 0.2
ξ_t	1.0 ± 0.2 km s^{-1}
$v \sin i$	1.6 ± 1.1 km s^{-1}
[Fe/H]	−0.08 ± 0.09
[Na/H]	0.07 ± 0.09
[Mg/H]	0.07 ± 0.16
[Al/H]	−0.01 ± 0.08
[Si/H]	0.05 ± 0.06
[Ca/H]	0.08 ± 0.15
[Sc/H]	0.01 ± 0.10
[Ti/H]	0.00 ± 0.10
[V/H]	0.06 ± 0.17
[Cr/H]	0.00 ± 0.05
[Mn/H]	0.00 ± 0.13
[Co/H]	−0.01 ± 0.07
[Ni/H]	−0.04 ± 0.06
log A (Li)	<0.5
Mass $M_\odot$	0.95 ± 0.09
Radius $R_\odot$	1.01 ± 0.26
Spectral type	G8 V
Distance	180 ± 60 pc

NOTE.—Mass and radius estimate using the Torres et al. (2010) calibration. Spectral type estimated from $T_{\rm eff}$ using the table in Gray (2008).

4. ROTATION PERIOD

The presence of Ca II H and K emission lines in the spectrum of WASP-41 suggests the possibility of variations in the light curve due to starspots with the same period as the rotation period of the star. The projected equatorial rotation velocity of WASP-41 combined with the estimated radius given in Table 2 imply a rotation period of 32 ± 23 days. We therefore searched for photometric variations in our WASP photometry with a similar period.

Our WASP photometry has a large number of observations (several thousand) with standard errors that vary from a few millimagnitudes for the best data up to a magnitude for data obtained on cloudy nights. WASP data obtained on cloudy nights is sometimes affected by large systematic errors, so we remove data with standard errors larger than five times the median value prior to further analysis. The remaining data still have a range of standard errors, so it is advantageous to use a period-searching algorithm that can account for this. The generalized Lomb-Scargle periodogram defined by Zechmeister and Kürster (2009) is a suitable method. However, there is little to be gained from including a "floating mean" in the case of the WASP data, so we used a slightly different definition of the periodogram equivalent to a least-squares fit of the sinusoidal function $y_i = a \sin(\omega t_i) + b \cos(\omega t_i)$ to magnitudes

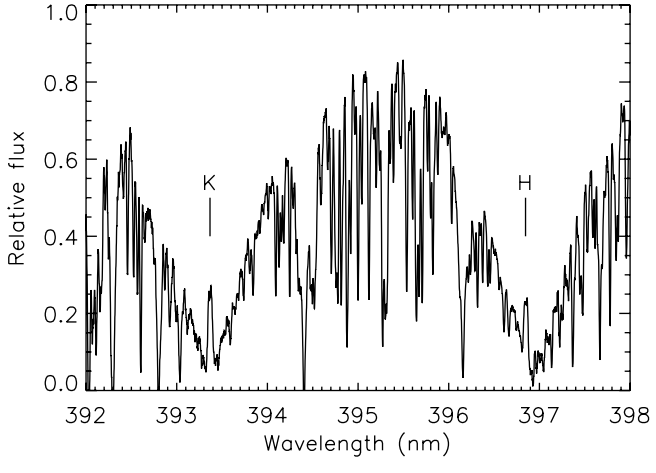

FIG. 3.—Section of the co-added Coralie spectra of WASP-41 showing emission in the core of the Ca II H and K lines.

$m_i = 1, 2, \ldots, N$ with standard errors σ_i obtained at times t_i for a given angular frequency ω. Note that we implicitly assume that the magnitudes m_i have a weighted mean value of 0. We used the following definition of the power at angular frequency ω:

$$P_n(\omega) = \frac{\chi_0^2 - \chi^2(\omega)}{\chi_0^2},$$

where

$$\chi_0^2 = \sum \frac{m_i^2}{\sigma_i^2}$$

and

$$\chi^2(\omega) = \sum \frac{(m_i - y_i)^2}{\sigma_i^2}.$$

We used this definition of the power to search for periodicity in the WASP-South light curves of WASP-41 at 4096 evenly spaced frequency values from 0 to 2.5 cycles day^{-1}. Variability due to starspots is not expected to be coherent on long timescales as a consequence of the finite lifetime of starspots and differential rotation in the photosphere, so we analyzed the two seasons of data for WASP-41 separately. The signal of the transits in the data was removed using a model similar to the one described subsequently, although, in practice, this has a negligible effect on the periodogram. We also analyzed three nearby stars of similar magnitude and color observed simultaneously with the same camera. The results are shown in Table 3. The periodograms of WASP-41 and one of the nearby stars are shown in Figure 4.

We used the method of Press and Rybicki (1989) to allow for fast and accurate computation of the periodogram. This enabled us to investigate the significance levels of any peaks in our periodograms using a bootstrap Monte Carlo approach. We generated synthetic data sets using a method similar to that devised by Collier Cameron et al. (2009), in which data are shuffled according to the date on which the data were obtained. The shuffling procedure shifts each night's observations in their entirety to a new date. This procedure effectively destroys coherent signals with periods longer than 1 day, but retains the global form of the window function and the effects of correlated noise. In addition to shuffling the date of the observations, we also change the sign of all the data from a given night for a random selection of half of the dates of observation.

Collier Cameron et al. (2009) use a single simulated data set to estimate the parameter $N_{\rm eff}$ in the following model for the distribution of power in the periodogram in the absence of any periodic signal:

$$\text{Prob}(P_n > P'_n) = (1 - P'_n)^{(N_{\rm eff}-3)/2}.$$

They then use this model to estimate the false-alarm probability (FAP) for the highest peak in the periodogram of the actual data from

$$\text{FAP} = 1 - [1 - \text{Prob}(P_n > P'_n)]^M,$$

where $M = (t_N - t_1)(f_{\rm max} - f_{\rm min})$ is an estimate of the number of independent frequencies in the periodogram calculated over the range of frequencies $f_{\rm min}$ to $f_{\rm max}$.[11] We found from simulations of a large number of data sets using both the "night-shuffling" method and Gaussian random noise that this method gives inaccurate estimates of FAP, particularly when this value is small. The principle reason for this is that the value of $N_{\rm eff}$ estimated from a single periodogram has a rather large uncertainty, typically around 20% for the data sets we investigated. We found that the following empirical model gives a good representation of the distribution of the peak power $P_{n,\rm best}$ in the periodograms we generated from simulated data:

$$\log_{10}[\text{Prob}(P_{n,\rm best} > P'_{n,\rm best})] = c_0 + c_1 P'_{n,\rm best} + c_2 (P'_{n,\rm best})^2.$$

For the analysis of a given set of data we use this model to fit the distribution of peak power values in 1024 simulated data sets. We then use the values of c_0, c_1, and c_2 to calculate the power corresponding to FAP $= 0.1$, 0.01, and 0.001 shown in Figure 4 and to estimate the FAP value for the highest peak in the actual periodogram given in Table 3.

There is a clear peak in the periodogram for WASP-41 near $P = 18$ days, although there appears to be a difference in the period derived from the two seasons of data (17.6 days and 18.4 days). We inspected the periodograms from the first season of data for WASP-41 and the three nearby stars and found that they all show power near 1 day, 30 days, and various combinations of these frequencies and their harmonics, presumably as a result of systematic errors in the photometry related to the diurnal and lunar cycles. In contrast, there is very little spurious power in the periodograms for the second season of data. For this reason, we identify the period of 18.41 ± 0.05 days derived from the second season of data as the correct rotation period for WASP-41. We estimated the standard error of the period measurement by analyzing 1024 data sets with the same number of points as the original sample, randomly resampled with reselection from the original data.

5. PLANETARY PARAMETERS

Our radial velocity (RV) and bisector span (BS) measurements for WASP-41 are shown in Figure 5 as a function of the photometric transit phase. There is a weak but statistically significant anticorrelation between these RV and BS values. In

[11] Note that there is an error in eq. (2) of Collier Cameron et al. (2009); the equation for FAP given here is the one actually used in that article.

TABLE 3
PERIOD ANALYSIS OF WASP-41 AND NEARBY STARS OF SIMILAR MAGNITUDE AND COLOR

Star	V	$B-V$	Year	N	RMS	$P_{\rm best}/d$	Power	FAP
WASP-41	11.6	0.7	2007	5673	0.041	17.62	0.358	2×10^{-5}
			2008	4966	0.019	18.41	0.240	6×10^{-7}
TYC 7247-1008-1	11.8	0.3	2007	5414	0.026	1.00	0.167	0.07
			2008	4834	0.012	0.98	0.023	0.65
TYC 7247-459-1	11.5	0.5	2007	5389	0.025	96.38	0.101	0.07
			2008	5003	0.012	1.62	0.006	0.45
TYC 7247-683-1	11.2	0.5	2007	5325	0.024	86.23	0.089	0.06
			2008	4993	0.012	0.46	0.005	1.00

principle, such an anticorrelation can be used to identify spurious RV signals caused by stellar activity. For example, Queloz et al. (2001) showed that the apparent RV signal in HD166435 is caused by stellar activity by identifying three characteristics of the signal:

1. The RV signal was not coherent over timescales of more than 30 days.
2. The amplitudes of the BS and RV variation were similar.
3. The BS variations were correlated with the photometric variations of the star.

In the case of WASP-41 there is no doubt that the RV signal is due to the presence of a planetary mass companion to WASP-41 and not due to stellar activity:

1. The RV signal is coherent over a timescale of more than 200 days.
2. The amplitude of the BS variation is an order of magnitude smaller than the RV variation.
3. The BS values are also correlated with the phase calculated for a rotation period of 18.4 days established from the photometric variations of WASP-41.

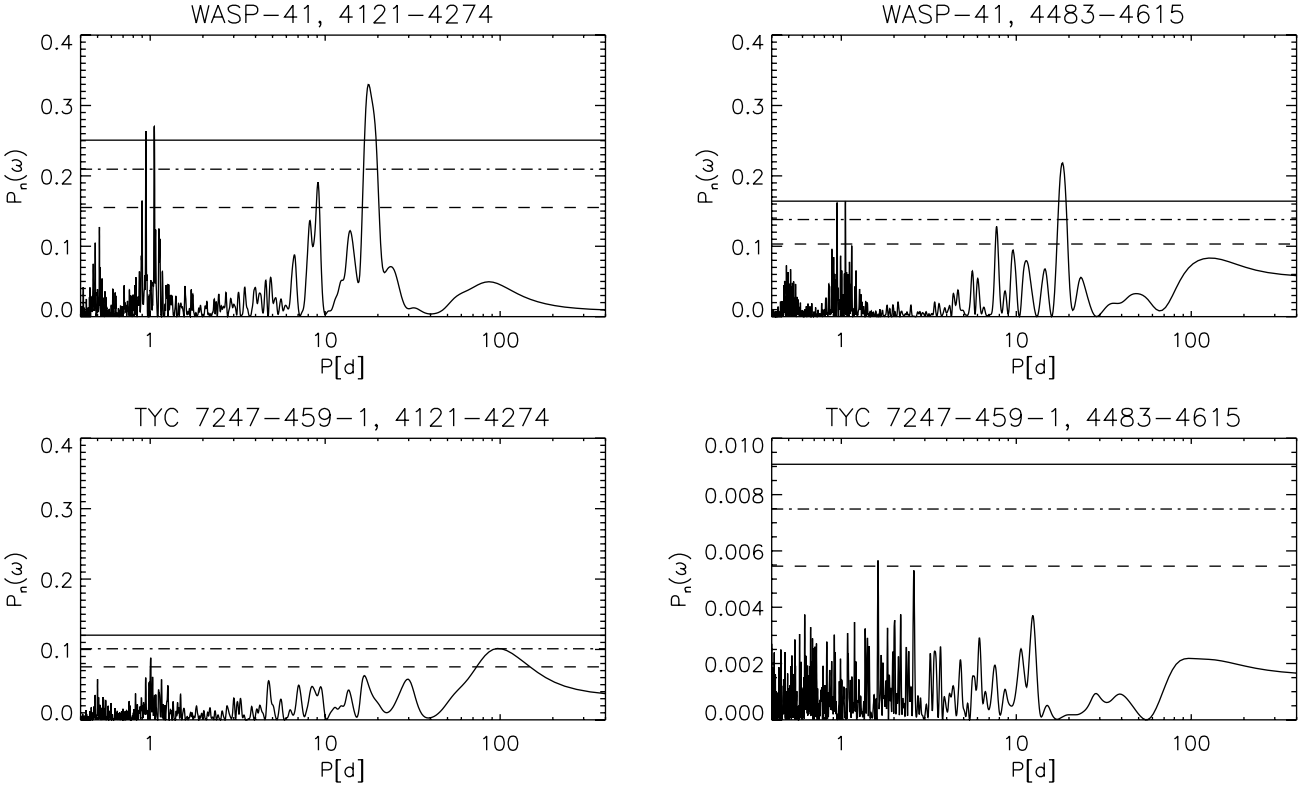

FIG. 4.—Periodogram of the WASP data from two seasons for WASP-41 and TYC 7247-459-1. The star name and date range (JD 245,000) are given in the title of each panel. Horizontal lines indicate false-alarm probability levels FAP = 0.1, 0.01, and 0.001. Note the change of scale in the lower right panel.

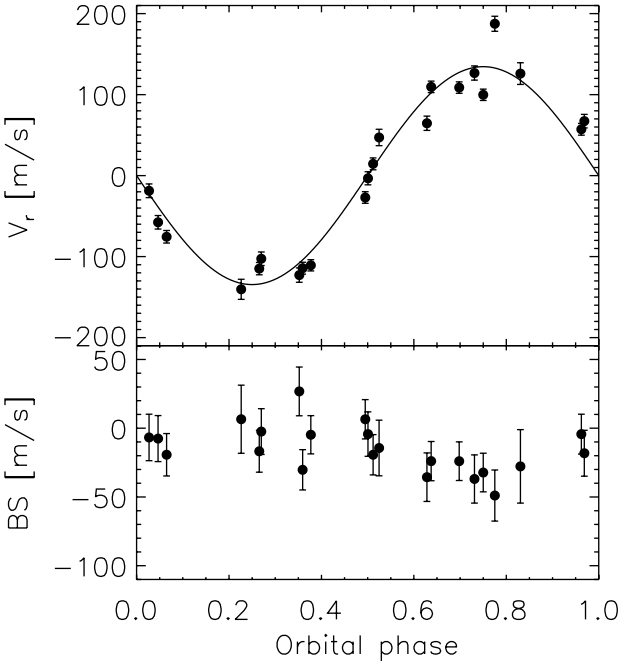

FIG. 5.—Radial velocity and bisector span measurements for WASP-41. *Top*: Radial velocity relative to the center-of-mass velocity together with the best-fit circular orbit. *Bottom*:: bisector span measurements.

As an additional test of the reality of the planetary RV signal, we also remeasured the RV values using a K5-type mask instead of a G2-type mask. Looking for a difference between the RV values derived with the different masks is an effective method for detecting spurious RV signals caused by starspots or faint eclipsing binary stars blended with the target star. In the case of WASP-41 there is no significant difference in the RV values measured with the two masks, so the best explanation for the observed RV and BS signals is that WASP-41 has a planetary mass companion with an orbital period of 3.05 days.

The Coralie radial velocity measurements were combined with the WASP-South and FTS photometry in a simultaneous Markov-chain Monte Carlo (MCMC) analysis to find the parameters of the WASP-41 system. We removed the photometric variation due to stellar rotation from the WASP-South photometry by subtracting a first-order harmonic series, fit by least-squares to the differential magnitudes from each season independently. The shape of the transit is not well defined in the WASP-South or FTS photometry, so we have imposed an assumed main-sequence mass-radius relation as an additional constraint in our analysis of the data. The stellar mass is determined from the parameters $T_{\rm eff}$, $\log g$, and [Fe/H] using the procedure described by Enoch et al. (2010), based on the compilation of eclipsing binary data by Torres et al. (2010). The code uses $T_{\rm eff}$ and [Fe/H] as MCMC jump variables, constrained by Bayesian priors based on the spectroscopically determined values given in Table 2. Limb-darkening coefficients are taken from Claret (2000).

The parameters derived from our MCMC analysis assuming a circular orbit are listed in Table 4. We found that the contribution to the value of χ^2 for the fit from the RV data was much higher than expected given the standard errors of these measurements. This is a result of additional noise in the RV data due to stellar activity (jitter). The free parameters in the fit to the RV are T_0, P, γ, and K, but the values of T_0 and P are determined almost entirely by the photometric data, so the number of degrees of freedom in the fit to the RV data is approximately 20. To achieve a contribution to the value of χ^2 from our 22 RVs of approximately 20, we found that we needed to add 21 $\rm m\,s^{-1}$ in quadrature to the standard errors for the RV data. We also performed an MCMC analysis of the data including the parameters $\sqrt{e}\cos\omega$ and $\sqrt{e}\sin\omega$ as free parameters. These parameters are used to describe an eccentric-orbit solution, because they are not strongly correlated and are equivalent to a assuming uniform prior distribution for the value of the eccentricity, e. With this eccentric-orbit solution and the same value of the jitter as the circular-orbit solution, we find $e = 0.10 \pm 0.06$. As this is consistent with a circular orbit, we adopt the parameters from the circular-orbit solution. As we do not know a priori that the orbit

TABLE 4
SYSTEM PARAMETERS FOR WASP-41

Parameter	Symbol	Value	Units
Transit epoch (HJD)	T_0	2,455,343.463 ± 0.001	Days
Orbital period	P	3.052401 ± 0.000004	Days
Planet/star area ratio[a]	$(R_p/R_*)^2$	0.0186 ± 0.0004	...
Transit duration	t_T	0.108 ± 0.002	Days
Impact parameter	b	$0.40^{+0.15}_{-0.11}$	R_*
Stellar reflex velocity	K_1	0.135 ± 0.008	$\rm km\,s^{-1}$
Center-of-mass velocity	γ	3.284 ± 0.009	$\rm km\,s^{-1}$
Orbital eccentricity	e	0 (fixed)	...
Orbital inclination	i	87.7 ± 0.08	°
Stellar density	$\rho_\star$	1.27 ± 0.14	$\rho_\odot$
Stellar mass	M_*	0.93 ± 0.03	$M_\odot$
Stellar radius	R_*	0.90 ± 0.05	$R_\odot$
Orbital semimajor axis	a	0.0402 ± 0.0005	AU
Planet radius[a]	R_p	1.20 ± 0.06	R_J
Planet mass	M_p	0.92 ± 0.06	M_J
Planet surface gravity	$\log g_p$	3.16 ± 0.04	cgs
Planet density	ρ_p	0.50 ± 0.08	ρ_J
Planet temperature	$T_{\rm eq}$	1230 ± 50	K

NOTES—.The planet equilibrium temperature is calculated assuming a value for the Bond albedo $A = 0$.

An assumed main-sequence mass-radius relation is imposed as an additional constraint in this solution, so the mass and radius of the star are not independent parameters—see Enoch et al. (2010) for details. Parameter values are taken for the solution assuming $e = 0$. Standard errors on the parameters are taken from the solution with $\sqrt{e}\cos(\omega)$ and $\sqrt{e}\sin(\omega)$ as free parameters

[a] These quantities may have a systematic error comparable with the random error due to the influence of stars spots on the FTS light curve.

is circular, we take the standard errors on the parameters from the noncircular-order solution.

We considered the contribution of correlated errors ("red noise") to the standard errors quoted in Table 4. While the individual transits in the WASP data are affected by red noise, the analysis of the combined light curve covering many individual transits will not be strongly affected by red noise, because there will be no correlation between the systematic noise from different nights. The FTS light curve is affected by red noise, so we have investigated the effect of this using the "prayer bead" method. A separate MCMC analysis was performed in which synthetic FTS light curves were created from the model fit to the light curve and the residuals from this model after cyclic permutation at each step in the MCMC chain. We find that this does not significantly increase the error estimates for any of the parameters.

Another issue to consider for the FTS light curve is the effect of starspots on the light curve, particularly given the sparse phase coverage of this light curve. Starspots can affect the parameters derived from this light curve in two ways. First, the normalization of the light curve can be affected by the overall change in brightness of the system due to the 18.4 day rotational modulation of the light curve. Second, small starspots covered by the planet during the transit by distort the shape of the light curve in a way that may be hard to spot by eye, but that introduce a systematic error in the parameters derived (Miller-Ricci et al. 2008). We have identified parameters in our solution that are determined primarily by the FTS light curve by performing an MCMC solution using the WASP and Coralie data only. We find that the depth of transit and the planet radius are the only parameters for which the standard error estimates increase significantly in the solution excluding the FTS data. In both cases, the values from the two solutions agree, but the solution excluding the FTS data has standard error estimates approximately twice as large as the solution including the FTS data. We conclude that these two parameters may be subject to systematic errors comparable with the random errors quoted in Table 4.

We have compared the values of the stellar effective temperature $T_{\rm eff}$ and the stellar density $\rho_\star$ with the stellar models of Girardi et al. (2000). We use the parameters $T_{\rm eff}$ and $\rho_\star$ because they are independently determined directly from the observations. We find that the mass inferred from the models ($0.9 \pm 0.1\ M_\odot$) is consistent with the mass derived in our MCMC analysis and that the uncertainties on the values of $T_{\rm eff}$ and $\rho_\star$ are too large for the models to provide any useful constraint on age of the star. The surface gravity derived from our MCMC solution is consistent with the $\log g$ value from the analysis of the spectrum, but the large uncertainty on the latter value means that this is a rather weak constraint.

6. DISCUSSION

WASP-41b joins a growing number of planets discovered with masses $\approx 0.9\ M_{\rm Jup}$ and radii $\approx 1.2\ R_{\rm Jup}$, orbiting solarlike stars with periods of about 3 days: e.g., HAT-P-13b XO-1b WASP-28b CoRoT-12b WASP-26b HAT-P-5b HAT-P-6b etc.[12] The WASP-41 planetary system is also similar to the TrES-1 system, particularly in regard to the activity level of the host star.

Knutson et al. (2010) suggest that there is a clear connection between the properties of the emission spectra from hot Jupiters and the activity levels of their host stars. In general, the emission spectrum of hot Jupiters measured from the eclipse depths at infrared wavelengths can only be matched by models that include a high-altitude temperature inversion. Four exceptions to this general rule are the planets orbiting the stars HD 189733, TrES-3, TrES-1, and WASP-4. Knutson et al. found that all four of these stars show moderate levels of chromospheric activity, higher than for all the other stars for which they were able to measure a value $\log R'_{\rm HK}$. The available evidence supports a hypothesis in which some source of optical opacity high in the atmosphere of hot Jupiter planets causes a temperature inversion, but that this opacity source is destroyed by the UV flux associated with chromospheric activity. The result found by Knutson et al. has a high statistical significance, but is based on a sample of only 15 stars. The situation is further complicated by the correlation between a planet's surface gravity and the level of chromospheric activity in its host star claimed by Hartman (2010). The values of $\log R'_{\rm HK}$ and $\log g_p$ we have measured for WASP-41 are consistent with the correlation observed by Hartman. The connection between chromospheric activity and temperature inversions can be confirmed in the case of WASP-41 using observations of the secondary eclipse with the IRAC instrument on the *Spitzer Space Telescope* at 3.6 μm and 4.5 μm (Knutson et al. 2010).

In principle, one can use an age/activity relation established from the average behavior of many solar-type stars to estimate the age of a star based on the measured $\log R'_{\rm HK}$ value. However, solar-type stars have activity cycles with periods of about a decade, during which the value of $\log R'_{\rm HK}$ can vary by 10% or more (Baliunas et al. 1995). This means that an age estimate based on a single measurement of $\log R'_{\rm HK}$ has an unknown systematic error that can be large enough to make the age estimate effectively meaningless. A more useful age estimate can be made in this case based on the observed rotation period of the star, $P_{\rm rot} = 18.4$ days. The calibration of the "gyrochronological" age given by Barnes (2007) implies an age of 1.8 Gyr for WASP-41, with an error of about 15%. Stars with $T_{\rm eff} =$ 5300–5600 K are seen to be lithium-poor in clusters with ages greater than 1 Gyr (such as NGC752 and M67), but the majority of stars in this $T_{\rm eff}$ range in clusters with ages of about 600 Myr (such as Praesepe), and the Hyades, NGC6633, and Coma Berenices are lithium-rich. We conclude that the upper limit to the lithium abundance given in Table 2 is consistent with any age greater than about 600 Myr (Sestito and Randich 2005).

[12] See http://exoplanet.eu.

WASP-South is hosted by the South African Astronomical Observatory and we are grateful for their ongoing support and assistance. Funding for the Wide Angle Search for Planets comes from consortium universities and from the UK's Science and Technology Facilities Council. We thank the referee for their careful reading of the article and for comments that improved the quality of this article.

REFERENCES

Baliunas, S. L., et al. 1995, ApJ, 438, 269
Barnes, S. A. 2007, ApJ, 669, 1167
Claret, A. 2000, A&A, 363, 1081
Collier Cameron, A., et al. 2007, MNRAS, 380, 1230
———. 2009, MNRAS, 400, 451
Enoch, B., Collier Cameron, A., Parley, N. R., & Hebb, L. 2010, A&A, 516, A 33
Gillon, M., et al. 2009, A&A, 496, 259
Girardi, L., Bressan, A., Bertelli, G., & Chiosi, C. 2000, A&AS, 141, 371
Gray, D. F. 2008, The Observation and Analysis of Stellar Photospheres, (Cambridge: Cambridge Univ. Press)
Hartman, J. D. 2010, ApJ, 717, L 138
Knutson, H. A., Howard, A. W., & Isaacson, H. 2010, ApJ, 720, 1569
Magain, P. 1984, A&A, 134, 189
Miller-Ricci, E., et al. 2008, ApJ, 682, 593
Noyes, R. W., Hartmann, L. W., Baliunas, S. L., Duncan, D. K., & Vaughan, A. H. 1984, ApJ, 279, 763
Pollacco, D., et al. 2008, MNRAS, 385, 1576
Pollacco, D. L., et al. 2006, PASP, 118, 1407
Press, W. H., & Rybicki, G. B. 1989, ApJ, 338, 277
Queloz, D., et al. 2001, A&A, 379, 279
———. 2000, A&A, 354, 99
Sestito, P., & Randich, S. 2005, A&A, 442, 615
Stetson, P. B. 1987, PASP, 99, 191
Torres, G., Andersen, J., & Giménez, A. 2010, A&A Rev., 18, 67
Wilson, D. M., et al. 2008, ApJ, 675, L 113
Zechmeister, M., & Kürster, M. 2009, A&A, 496, 577